



HAL
open science

Pressure-induced incommensurate antiferromagnetic order in a ferromagnetic B-site ordered double-perovskite Lu₂NiMnO₆

Noriki Terada, Claire Colin, Navid Qureshi, Thomas C Hansen, Kazuyuki Matsubayashi, Yoshiya Uwatoko, Alexei A Belik

► **To cite this version:**

Noriki Terada, Claire Colin, Navid Qureshi, Thomas C Hansen, Kazuyuki Matsubayashi, et al.. Pressure-induced incommensurate antiferromagnetic order in a ferromagnetic B-site ordered double-perovskite Lu₂NiMnO₆. *Physical Review B*, 2020, 102 (9), pp.094412. 10.1103/physrevb.102.094412 . hal-04143373

HAL Id: hal-04143373

<https://hal.science/hal-04143373>

Submitted on 27 Jun 2023

HAL is a multi-disciplinary open access archive for the deposit and dissemination of scientific research documents, whether they are published or not. The documents may come from teaching and research institutions in France or abroad, or from public or private research centers.

L'archive ouverte pluridisciplinaire **HAL**, est destinée au dépôt et à la diffusion de documents scientifiques de niveau recherche, publiés ou non, émanant des établissements d'enseignement et de recherche français ou étrangers, des laboratoires publics ou privés.

Pressure-induced incommensurate antiferromagnetic order in a ferromagnetic B -site ordered double-perovskite $\text{Lu}_2\text{NiMnO}_6$

Noriki Terada ^{1,*}, Claire V. Colin,² Navid Qureshi,³ Thomas C. Hansen ³, Kazuyuki Matsubayashi,^{4,5} Yoshiya Uwatoko,⁵ and Alexei A. Belik ⁶

¹National Institute for Materials Science, Sengen 1-2-1, Tsukuba, Ibaraki 305-0047, Japan

²Université Grenoble Alpes, CNRS, Institut Néel, 38042 Grenoble, France

³Institut Laue-Langevin, Boîte Postale 156, F-38042, Grenoble Cedex 9, France

⁴Department of Engineering Science, University of Electro-Communications, Chofu, Tokyo 182-8585, Japan

⁵Institute for Solid State Physics, University of Tokyo, Kashiwanoha 5-1-5, Kashiwa, Chiba 277-8581, Japan

⁶International Center for Materials Nanoarchitectonics (WPI-MANA), National Institute for Materials Science (NIMS), Namiki 1-1, Tsukuba, Ibaraki 305-0044, Japan



(Received 27 May 2020; revised 28 July 2020; accepted 27 August 2020; published 9 September 2020)

We have investigated the pressure effect on magnetic ordering of the ferromagnetic double perovskite $\text{Lu}_2\text{NiMnO}_6$ by magnetization, ac magnetic susceptibility, and neutron diffraction experiments up to 8.0 GPa in order to understand the ferromagnetic-to-antiferromagnetic phase transition by substitution of the A sites in $A_2\text{NiMnO}_6$ from rare-earth to indium or scandium ions. Strong ferromagnetic spin correlation seen in the susceptibility at low pressure is significantly suppressed by increasing pressure. In a neutron diffraction experiment, the magnetic Bragg reflections associated with ferromagnetic ordering disappear above 4.5 GPa. For the high-pressure region above 4.5 GPa, an antiferromagnetic ordering with long-period incommensurate modulation appears, which is coexistent with ferromagnetic short-range order. From mean-field calculations, we infer that pressure modification of the delicate balance of the competing next-nearest-neighbor exchange interactions between Ni and Ni, or Mn and Mn, plays an important role in the phase transition from ferromagnetic to antiferromagnetic ordering in $A_2\text{NiMnO}_6$.

DOI: [10.1103/PhysRevB.102.094412](https://doi.org/10.1103/PhysRevB.102.094412)

I. INTRODUCTION

Ordered double perovskite oxides with the chemical composition $A_2B'B''O_6$ (A is an alkaline-earth ion, Y, or a rare-earth ion) have been studied extensively since the 1960s [1–3]. Since the B' and B'' sites are occupied by transition-metal ions, they exhibit various types of spin-related physical phenomena as a result of coupling between spin and another degree of freedom of electrons [4,5]. Magnetolectric multiferroic phenomena have attracted much attention in the past 15 years, since the discovery of magnetic-field-controlled ferroelectricity in TbMnO_3 [6–8]. The multiferroic behavior has been investigated for various types of crystal structure in order to understand the mechanism regarding spin-order-induced ferroelectricity and with the goal of practical application. Double perovskite compounds have been studied as multiferroics much less frequently due to the use of a simple ferromagnet in most cases, which does not significantly affect the ferroelectricity. Nevertheless, there are several exceptions to antiferromagnetic (AFM) ordering in double perovskites $A_2\text{MnCoO}_6$ ($A = \text{Yb, Lu}$) [9,10] and $A_2\text{NiMnO}_6$ ($A = \text{In, Sc}$) [11–14] with a relatively small ionic radius of the A sites. Spin-order-driven ferroelectricity has been reported in a

$\uparrow\uparrow\downarrow\downarrow$ structure in $\text{Lu}_2\text{MnCoO}_6$ [10], and a long-period spiral ordering has been reported in $\text{In}_2\text{NiMnO}_6$ [13].

In $A_2\text{NiMnO}_6$, since the nearest-neighbor exchange interaction between Ni^{2+} and Mn^{4+} is expected to be ferromagnetic (FM) in the Kanamori-Goodenough (KG) rule [15,16], all the compounds with the A site occupied by rare-earth elements or Y are FM [17–19]. Decreasing the ionic radius of the A sites in $A_2\text{NiMnO}_6$ makes the bond angle of Ni-O-Mn far from 180° and reduces the FM interactions, which is proved by the decrease of the Curie temperature from $T_c \simeq 300$ K for $\text{La}_2\text{NiMnO}_6$ to $T_c \simeq 45$ K for $\text{Lu}_2\text{NiMnO}_6$ (Fig. 1) [17–19]. Further compression of the ionic size has been successful for $A = \text{In}$ and Sc by using high-pressure and high-temperature synthesis techniques [11,12]. In the smallest A -site cation case of $\text{Sc}_2\text{NiMnO}_6$, a multi- k AFM ordering with commensurate propagation vectors $\mathbf{k} = (\frac{1}{2}, 0, \frac{1}{2})$ and $(0, \frac{1}{2}, \frac{1}{2})$ is found as the magnetic ground state, which does not induce ferroelectricity [14]. However, for compounds with the ionic sizes between Sc and Lu, i.e., $\text{In}_2\text{NiMnO}_6$, there exists a complex spiral phase (Fig. 1). The ferroelectric polarization with $\sim 30 \mu\text{C}/\text{m}^2$ is induced by the complex spiral ordering with an incommensurate (ICM) $\mathbf{k} = (0.274, 0, -0.0893)$ in $\text{In}_2\text{NiMnO}_6$ [13].

Several theoretical studies for $A_2\text{NiMnO}_6$ have predicted that the Ni-O-Mn exchange interaction changes from FM to AFM with decreasing ionic radius of the A sites, and the $\uparrow\uparrow\downarrow\downarrow$ AFM structure in Y_2NiMnO_6 [20] and $\text{In}_2\text{NiMnO}_6$ [11] would be stable. The predictions, however, were not in

*TERADA.Noriki@nims.go.jp

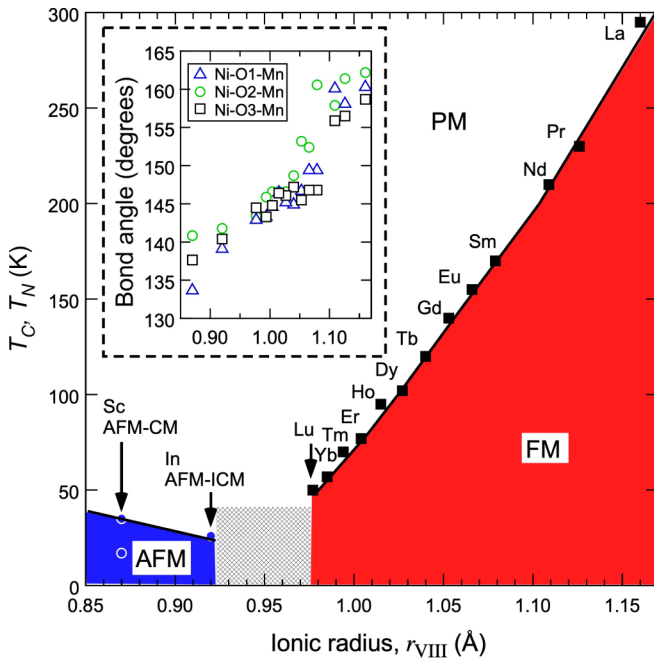


FIG. 1. Magnetic phase diagram of A_2NiMnO_6 as functions of temperature and ionic radius. The phase-transition temperature points are taken from previous papers [17–19]. The hatched area denotes the phase boundary between ferromagnetic (FM) and antiferromagnetic (AFM) phases. The inset shows the ionic radius dependence of bond angles, Ni-O1-Mn, Ni-O2-Mn, and Ni-O3-Mn.

agreement with the experimental results of FM Y_2NiMnO_6 [21] and the ICM order in In_2NiMnO_6 [13]. Therefore, it is still an open question as to which exchange interactions are important for the drastic change in the magnetic ordering in A_2NiMnO_6 . Seeing the relationship between the lattice volume and magnetic phase transitions in A_2NiMnO_6 , we realized that the difference in the volume between FM Lu_2NiMnO_6 (LNMO) and AFM In_2NiMnO_6 is nearly 1%. Such a volume change is normally reachable by application of hydrostatic pressure on the order of several GPa [22]. We thus anticipate that it can be possible to study the phase transition from the FM phase to the AFM phase by continuously changing the lattice parameters by application of pressure in LNMO. In this study, we investigate the pressure effect on the magnetic ordering in FM LNMO by magnetization, magnetic susceptibility measurements, and a neutron diffraction experiment under high-pressure conditions.

II. EXPERIMENTAL DETAILS

A polycrystalline sample of LNMO was prepared from a stoichiometric mixture of Lu_2O_3 , NiO, and Mn_2O_3 with the addition of a small amount of $KClO_4$ as an oxidizer. The mixture was placed in a Pt capsule and treated at 6 GPa and about 1770 K for 2 h (heating time to the synthesis temperature was 10 min) in a belt-type high-pressure apparatus in the National Institute for Materials Science. After the heat treatment, the sample was quenched to room temperature (RT) and the pressure was slowly released. The resultant sample was washed in warm water to remove KCl impurity formed after the

decomposition of $KClO_4$. X-ray powder diffraction (XRPD) data were collected at RT on a RIGAKU RINT2000 diffractometer using $Cu K\alpha$ radiation. The sample was single-phase, and refined lattice parameters were $a = 5.1482(2)$ Å, $b = 5.5151(2)$ Å, $c = 7.4076(3)$ Å, and $\beta = 90.448(1)^\circ$ (space group $P2_1/n$). The atomic disorder between Ni and Mn atoms was not observed in the present x-ray and neutron diffraction data.

For the dc magnetization measurements, the magnetic properties measurement system MPMS manufactured by Quantum Design was used. For generating high pressure, we used a piston-cylinder-type high-pressure cell (LPC-15, ElectroLAB Company). A powder sample with a mass of 9 mg was put into a Teflon capsule with a glycerin pressure transmission medium. The pressure was determined by measuring the superconducting phase transition of Pb. The accuracy of the pressure determination for the dc measurements was not worse than ± 0.05 GPa.

For the ac magnetic susceptibility measurements, high pressure was generated using a cubic anvil high-pressure apparatus consisting of six tungsten carbide anvils, which has been proved to produce a homogeneous pressure [23]. The pressure of the sample is calibrated by measurement of the resistivity changes of Bi and Te associated with their structural phase transitions at room temperature. The accuracy of the pressure determination for the ac measurements was not worse than ± 0.1 GPa. The force applied to the sample is kept constant during the measurement by cooling and warming runs. We use glycerin and pyrophyllite as the pressure-transmitting medium and the gasket, respectively. The ac magnetic susceptibility was measured using a conventional Hartshorn bridge circuit at a fixed frequency of 317 Hz. A modulation field with an amplitude of 2 Oe was applied.

A neutron diffraction experiment under high pressure was performed with the D20 two-axis diffractometer at Institut Laue Langevin in Grenoble, France [24]. An incident neutron wavelength of 2.41 Å was employed. We used a Paris-Edinburgh (PE) press with sintered diamond anvils, called SINE anvils, and a helium bath cryostat for the high-pressure and low-temperature sample environment [25]. The powder sample and some pieces of Pb were put into a Ti-Zr alloy gasket filled with a pressure transmission medium composed of a deuterated 4:1 methanol-ethanol mixture. The pressure was estimated from the scattering angle for the (200) Bragg peak of Pb by referring to the known pressure and temperature dependence [25]. The accuracy of the pressure determination was nearly ± 0.5 GPa. The magnetic structure analysis, including Rietveld refinement, was carried out using the FULLPROF SUITE program [26].

III. EXPERIMENTAL RESULTS

A. Magnetization and ac magnetic susceptibility

Results for the dc magnetization measurements in LNMO are shown in Fig. 2(a). At ambient pressure, the magnetization starts to grow at $T \simeq 36$ K upon cooling, which is slightly lower than $T_c = 45$ K reported in a previous paper [17]. This may be a result of the difference in oxygen stoichiometry, which is seen in La_2NiMnO_6 [27]. The magnetization at 2.0 K

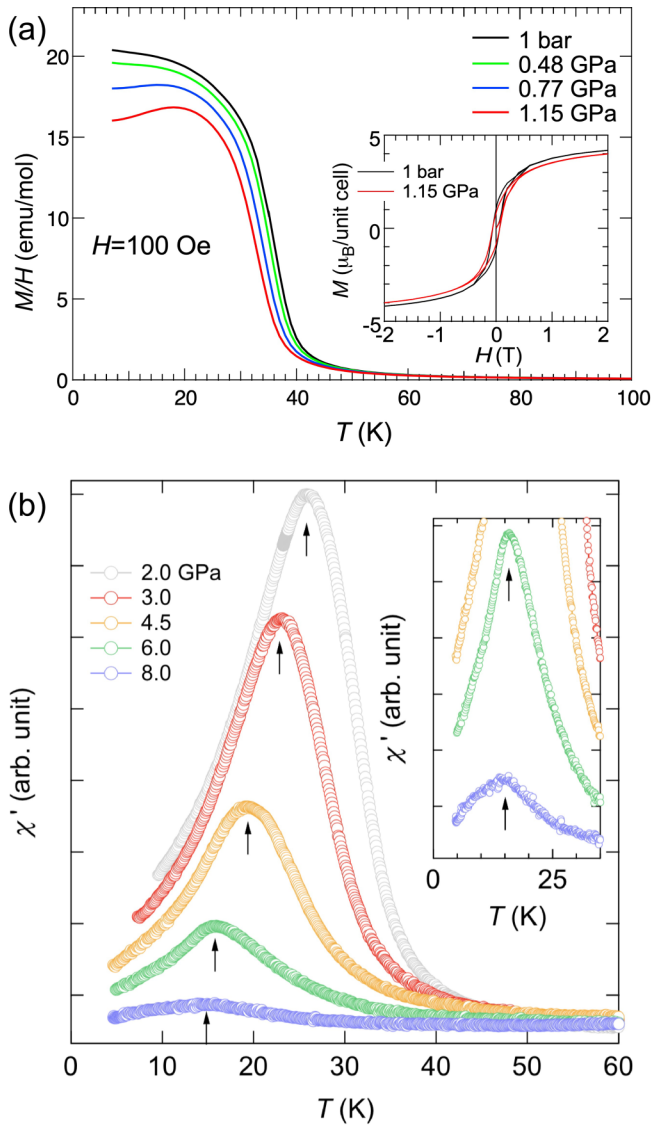


FIG. 2. Temperature dependences of (a) dc magnetization and (b) the real part of magnetic susceptibility for typical pressures in $\text{Lu}_2\text{NiMnO}_6$. The insets in (a) and (b) show the magnetic field variation of the magnetization at $T = 2.0$ K and the magnification for the high-pressure data, respectively.

exhibits a typical FM hysteresis curve as a function of the magnetic field, as shown in the inset of Fig. 2(a). Application of pressure changes the phase-transition temperature, at which dM/dT shows a local minimum, from 36 to 33 K at $P = 1.15$ GPa. The magnetization at $P = 1.15$ GPa slightly decreases below ~ 20 K, indicating the reduction of FM interaction with increasing pressure. In fact, the Curie-Weiss (CW) temperature, estimated by CW fitting of the data for $100 \leq T \leq 300$ K, is also slightly changed from $\Theta_{\text{CW}} = 54.9$ K at ambient pressure to $\Theta_{\text{CW}} = 52.2$ K at $P = 1.15$ GPa. The M - H curves at ambient pressure and $P = 1.15$ GPa are almost identical, apart from a slight difference in saturation magnetization.

The temperature dependence of the ac magnetic susceptibility, χ' (real part of complex susceptibility), at typical pressures $P \geq 2.0$ GPa for LNMO is shown in Fig. 2(b). A

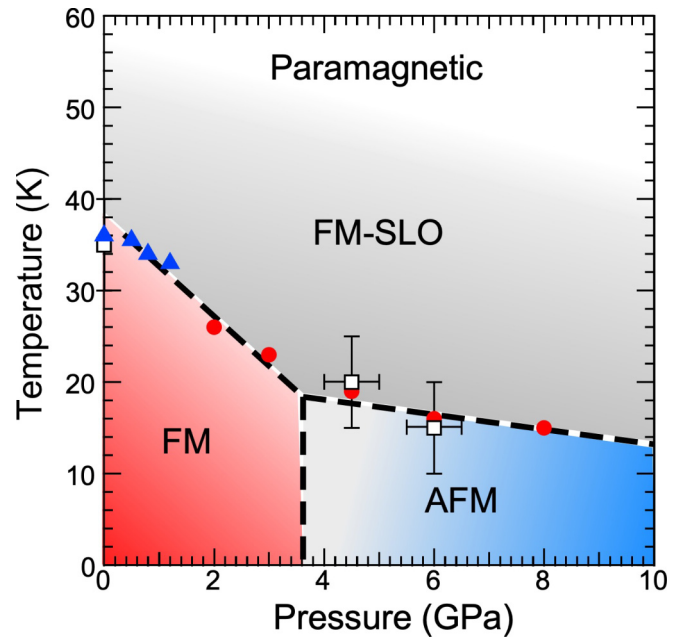


FIG. 3. Temperature vs pressure magnetic phase diagram for $\text{Lu}_2\text{NiMnO}_6$. Triangle, circle, and square symbols denote the magnetic phase transitions determined by the dc magnetization, ac magnetic susceptibility, and neutron diffraction experiments, respectively.

large peak is observed at $T = 26$ K and $P = 2.0$ GPa. This peak is typically seen for a phase transition from paramagnetic to FM [28], and it reflects significant FM fluctuation around the phase transition. With increasing pressure, the large peak is shifted toward lower temperature and the peak height is significantly reduced. This indicates that the FM fluctuation observed at lower pressure is largely suppressed by application of pressure.

The pressure dependence of the phase-transition temperature is plotted as a phase diagram in Fig. 3. Significant reduction of the phase-transition temperature is seen below ~ 4.0 GPa, while the tendency becomes much less above this pressure. Considering that the FM fluctuation is suppressed with increasing pressure and almost disappears at 8.0 GPa, we can infer that the magnetic ground state is changed from FM to AFM around ~ 4.0 GPa.

B. Neutron diffraction

1. Ambient pressure

For comparison with the results under high pressure, we first performed neutron diffraction measurements at ambient pressure with the identical experimental setup where the sample was put into the PE press. The data shown in Fig. 4 are subtracted by the data measured in the paramagnetic phase at $T = 80$ K. Even for the high-temperature region above $T_c = 36$ K, a diffuse magnetic signal is observed in the low- Q region, $Q \leq 0.4 \text{ \AA}^{-1}$ in the paramagnetic phase, which corresponds to the existence of FM short-range order (SLO). Additional peaks with a width corresponding to the instrumental resolution, which indicates magnetic long-range

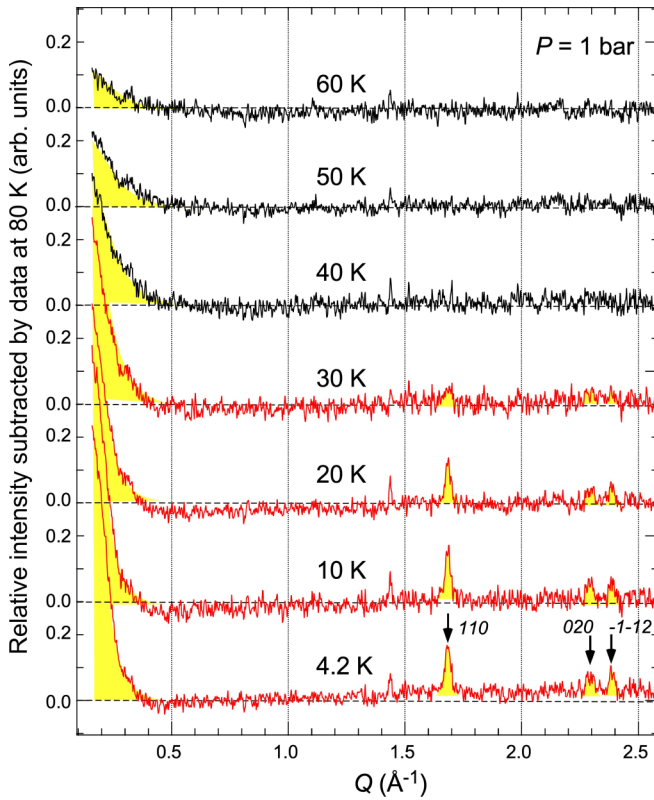


FIG. 4. Temperature dependence of neutron diffraction profiles at ambient pressure in $\text{Lu}_2\text{NiMnO}_6$. The data are subtracted by those measured at $T = 80$ K. Arrows denote the positions of magnetic Bragg reflections.

order, appear below $T_c = 36$ K. The sharp peaks are indexed by $\mathbf{k} = (0, 0, 0)$.

To determine the magnetic structure at $T = 4.2$ K and ambient pressure, we performed a magnetic structure analysis with symmetry analysis. There are two magnetic one-dimensional irreducible representations (IRs) for $\mathbf{k} = (0, 0, 0)$ in the $P2_1/n$ space group: $m\Gamma_1^+$ and $m\Gamma_2^+$ [29]. In the $m\Gamma_1^+$, the spin projection in the ac -plane is an AFM arrangement and the b -component is an FM arrangement, whereas the former is an FM arrangement and the latter is antiferromagnetic in the $m\Gamma_2^+$. Taking the observation of the 020 -reflection into account, the spin ac -plane component should be ferromagnetic, which excludes the $m\Gamma_1^+$ possibility. We refined the spin orientation parameters as Mn and Ni spins are independent for $m\Gamma_2^+$. These parameters are almost the same within the experimental accuracy. We thus fixed the spin directions to be the same for Ni and Mn spins in this refinement. As shown in Fig. 5(a), the calculated intensities for some magnetic Bragg peaks are in good agreement with the experimental data. The refined spin components are $\mathbf{M}(\text{Ni}) = (1.1(6), 0, 1.6(3)) \mu_B$ and $\mathbf{M}(\text{Mn}) = (1.5(8), 0, 2.2(5)) \mu_B$. The nonzero spin b -component does not improve the refinement. The determined magnetic structure is illustrated in Fig. 5(b). The spin canting angle is $\sim 36^\circ$ from the c -axis in the ac -plane, which is almost parallel to the $[1,0,1]$ direction in real space. The magnetic structure belongs to the $P2_1'/n'$ magnetic space group.

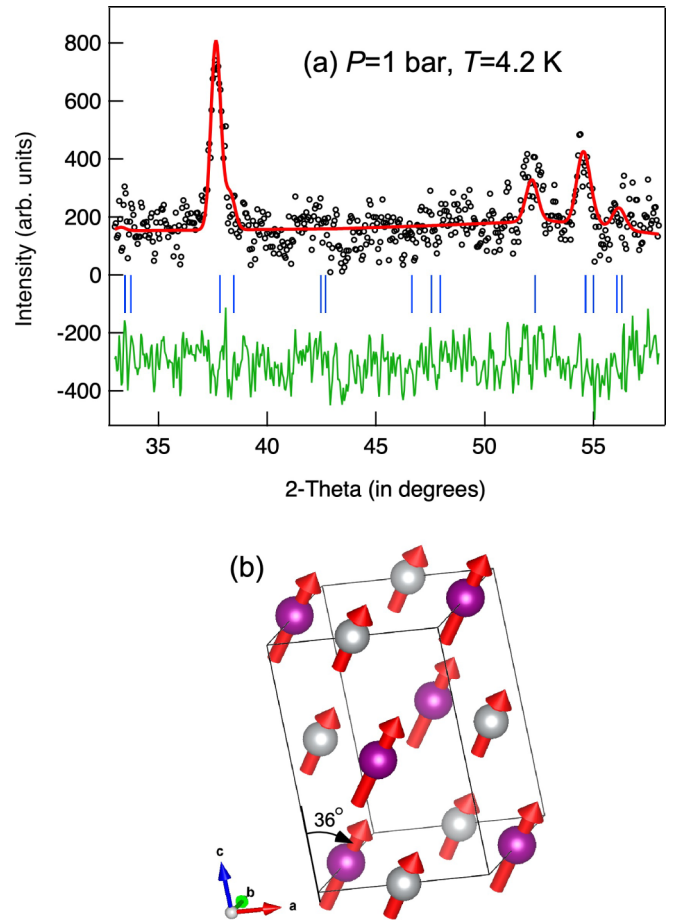


FIG. 5. (a) Result of the Rietveld refinement for the data at $T = 4.2$ K and ambient pressure. The experimental data are subtracted by those at $T = 80$ K. Circles and thick and thin lines denote the observed data, calculated data, and the difference between the data, respectively. The vertical bars are the symmetry-allowed magnetic Bragg positions. (b) Illustration of the determined magnetic structure at ambient pressure in $\text{Lu}_2\text{NiMnO}_6$.

2. High-pressure region

For $P = 6.0$ GPa, the temperature dependence of the neutron diffraction profile, which is subtracted by the data at $T = 80$ K and $P = 6.0$ GPa, is shown in Fig. 6. As seen in the result at ambient pressure (Fig. 4), the magnetic signal corresponding to the FM SLO is also observed at $P = 6.0$ GPa. However, no sharp Bragg reflections are observed even below the phase-transition temperature, $T = 16$ K ($\equiv T_N$), which is determined in the magnetic susceptibility measurement. For the data at $T = 10$ K and 4.2 K, there is a small kink observed at $Q \sim 0.3 \text{ \AA}^{-1}$, as indicated by an arrow in Fig. 6. We can infer that a long-period AFM ordering coexists with the FM SLO below $T_N = 16$ K.

For extracting only the AFM component seen in the low- Q region from the low-temperature data, the data at $T = 4.2$ K were subtracted by the data at 20 K near the transition temperature. This can exclude the FM SLO component from the low-temperature data. Figure 7 shows the relative intensity at $T = 4.2$ K for $P = 1$ bar, $P = 4.5$ GPa, and $P = 6.0$ GPa, which are subtracted by the data at $T = 50$ K, 25 K, and

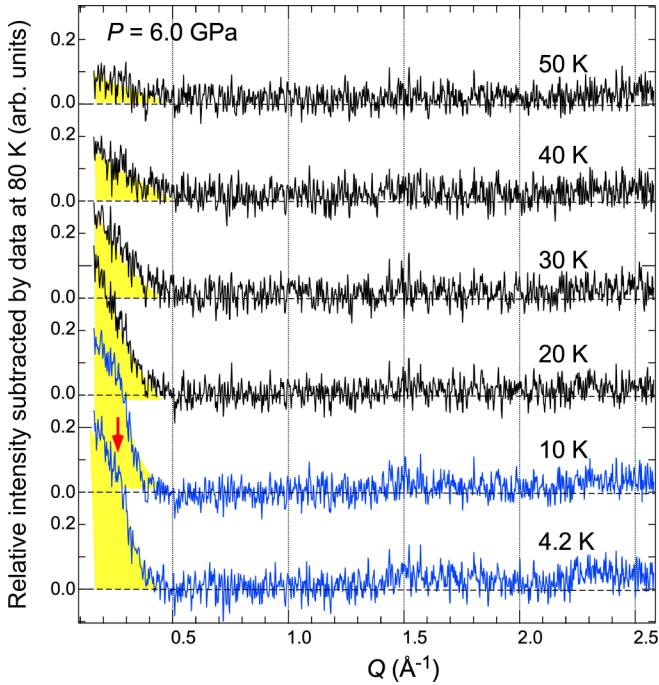


FIG. 6. Temperature dependence of neutron diffraction profiles. The data are subtracted by the data at $T = 80$ K and $P = 6.0$ GPa. The arrow indicates the position of the antiferromagnetic signal, which is described in the main text.

20 K, respectively. We observe a peak at $Q \simeq 0.24 \text{ \AA}^{-1}$ for $P = 6.0$ GPa, which corresponds to an AFM order with a long period of 26.2 \AA . We did not see other magnetic peaks at high-pressure data in the present experiment for LNMO. For the similar ICM ordering in $\text{In}_2\text{NiMnO}_6$, the second peak is estimated to be as large as $\sim 7\%$ of the first peak [13]. Therefore, the observation of the second peak is beyond the experimental

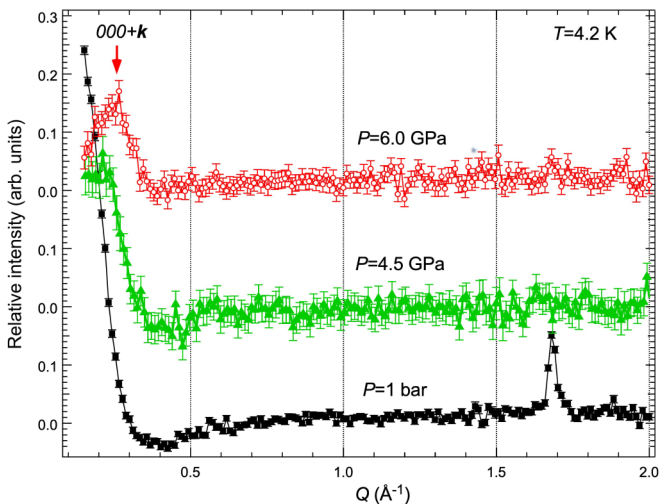


FIG. 7. The neutron diffraction profiles at $T = 4.2$ K and $P = 1$ bar, $P = 4.5$ GPa, and $P = 6.0$ GPa, which are subtracted by the data at 50, 25, and 20 K, respectively. The inset shows the magnification of the data around $Q \sim 0.17 \text{ \AA}^{-1}$ at $T = 4.2$ K and $P = 6.0$ GPa.

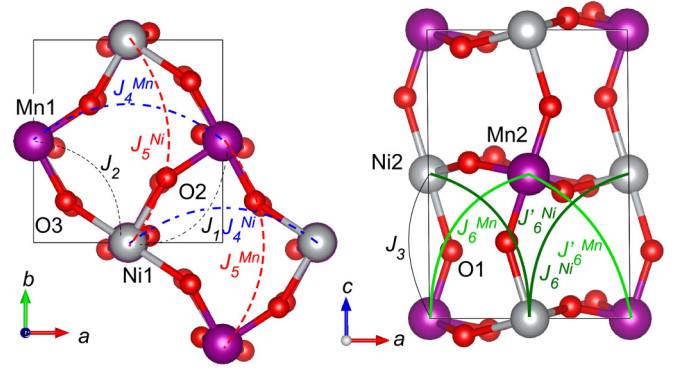


FIG. 8. Illustration of the exchange interaction paths bonding two spins of atoms, (1)Mn1(0,1/2,0), (2)Ni1(1/2,0,0), (3)Mn2(1/2,0,1/2), and (4)Ni2(0,1/2,1/2).

resolution in the present experiment. From only one observable reflection, we could not determine the \mathbf{k} -vector in the high-pressure phase of LNMO. Assuming that the \mathbf{k} -vector is parallel to that of $\text{In}_2\text{NiMnO}_6$, $\mathbf{k} = (0.274, 0, -0.0893)$, it would be $\mathbf{k} = (0.184, 0, -0.060)$ at $P = 6.0$ GPa in LNMO. To determine the \mathbf{k} -vector in LNMO precisely, a further neutron diffraction experiment with a single crystal (or a higher-quality experiment with a powder sample) is needed.

IV. DISCUSSION

Let us discuss the relationship between the pressure dependence of the lattice parameters and the magnetic order in LNMO. The lattice parameters for ambient pressure and $P = 6.0$ GPa are listed in Table I. For comparison with other double perovskites with similar lattice parameters, $A_2\text{NiMnO}_6$ ($A = \text{Y, In, Sc}$) are also shown in the table. The unit cell volume (V) for LNMO is compressed from $210.204(11) \text{ \AA}^3$ at ambient pressure to $204.875(15) \text{ \AA}^3$ at $P = 6.0$ GPa. The V value at $P = 6.0$ GPa in LNMO is between those for $\text{In}_2\text{NiMnO}_6$ with AFM-ICM and $\text{Sc}_2\text{NiMnO}_6$ with an AFM-CM ground state. Therefore, the average exchange bond lengths expected from the V value are expected to give an AFM ground state, as also seen in the phase diagram shown in the Introduction (Fig. 1).

Which exchange interactions are important for understanding the pressure-induced phase transition from FM to AFM-ICM states seen in LNMO? We consider the nearest-neighbor (NN) interactions for Ni-O-Mn bonds (J_1, J_2, J_3) and the next-nearest-neighbor (NNN) interactions for Ni-O-O-Ni bonds ($J_4^{\text{Ni}}, J_5^{\text{Ni}}, J_6^{\text{Ni}}, J_6^{\text{Ni}}$) and Mn-O-O-Mn bonds ($J_4^{\text{Mn}}, J_5^{\text{Mn}}, J_6^{\text{Mn}}, J_6^{\text{Mn}}$). These exchange interaction paths are illustrated in Fig. 8 and are listed in Table II. For the NN interactions, according to the KG rule, superexchange interaction between Ni^{2+} and Mn^{4+} bonded by O^{2-} (Ni-O-Mn) with bond angle 180° is FM. Although the bond angle is not 180° but $\sim 140^\circ$ in LNMO, the FM interaction is expected to be weaker than in the case of the 180° bond, which is proved by the decrease in T_c with reducing the bond angles (see the inset of Fig. 1). This was also suggested by previous density-functional calculations for Y_2NiMnO_6 , where the Ni-O-Mn interactions are FM [20]. As shown in Table I, the bond angles

TABLE I. List of lattice constants, angles, and distances for some exchange interaction bond for $\text{Lu}_2\text{NiMnO}_6$ (ambient pressure and 6.0 GPa), and other $A_2\text{NiMnO}_6$ ($A = \text{Y, In, Sc}$). The symmetry is $P2_1/n$ with $A = (\text{Lu, Y, In, Sc})$, Ni, Mn, and O at the Wyckoff positions, $4e$ (x, y, z), $2d$ ($1/2, 0, 0$), $2c$ ($1/2, 0, 1/2$), and $4e$ (x, y, z), respectively. The exchange interaction paths, J_n ($n = 1-6$), are described in the main text.

Magnetic ground state	$\text{Lu}_2\text{NiMnO}_6$ ($P = 1$ bar) FM	$\text{Lu}_2\text{NiMnO}_6$ ($P = 6.0$ GPa) AFM (ICM)	Y_2NiMnO_6 Ref. [21] FM	$\text{In}_2\text{NiMnO}_6$ Ref. [11] AFM (ICM)	$\text{Sc}_2\text{NiMnO}_6$ Ref. [14] AFM (CM)
Temperature (K)	80 (300)	80	300	300	300
a (Å)	5.14851(15) [5.1563(2)]	5.1016(2)	5.2267(3)	5.13520(1)	4.99860(2)
b (Å)	5.51541(15) [5.5183(2)]	5.4733(2)	5.5582(6)	5.33728(1)	5.35281(2)
c (Å)	7.4028(3) [7.4144(4)]	7.2275(3)	7.4835(2)	7.54559(4)	7.34496(2)
β (deg)	90.498(3) [90.443(5)]	90.533(4)	90.294(45)	90.1343(1)	90.7915(2)
V (Å ³)	210.204(11) [210.966(16)]	204.875(15)	217.401	206.809(5)	196.5068(11)
$\angle_{\text{Ni-O1-Mn}}$	143.0(3) [143.8(4)]	143.7(3)	145.5	139.1(1)	133.7(1)
$\angle_{\text{Ni-O2-Mn}}$	146.6(3) [146.8(5)]	148.5(4)	145.5	141.8(2)	140.8(1)
$\angle_{\text{Ni-O3-Mn}}$	144.6(3) [144.4(4)]	142.4(4)	146.3	140.4(2)	137.7(1)
$J_1, J_2 : d_{\text{Ni-Mn}}^{110}$	3.77250(8) [3.77621(11)]	3.74110(11)	3.81484	3.70327	3.66192
$J_3 : d_{\text{Ni-Mn}}^{001}$	3.70140(16) [3.7072(3)]	3.66875(16)	3.74175	3.77279(2)	3.67248
$J_4 : d_{\text{Ni-Mn}}^{100}$	5.14851(15) [5.1563(2)]	5.1016(2)	5.2267(3)	5.13520(1)	4.99860(2)
$J_5 : d_{\text{Ni-Mn}}^{010}$	5.51541(15) [5.5183(2)]	5.4733(2)	5.5582(6)	5.33728(1)	5.35281(2)
$J_6 : d_{\text{Ni-Ni(Mn-Mn)}}^{111}$	5.26939(16) [5.2778(3)]	5.22316(18)	5.35295	5.28231	5.16170
$J'_6 : d_{\text{Ni-Ni(Mn-Mn)}}^{11-1}$	5.30073(16) [5.3057(3)]	5.25639(18)	5.33417	5.29090	5.21060

TABLE II. Relationship between atom positions in the unit cell for Mn and Ni ions in the monoclinic $P2_1/n$ space group, and exchange interaction parameters.

Atom (site)	No.	x, y, z	J : Neighbor no. (lattice translation)
Mn1(2c)	1	(0,1/2,0)	$J_1:2(1,0,0), J_2:2(0,0,0), J_3:4(0,0,0), J_4^{\text{Mn}}:1(1,0,0), J_5^{\text{Mn}}:1(0,1,0), J_6^{\text{Mn}}:3(0,0,0), J_6^{\text{Mn}}:3(1,0,1), J_6^{\text{Mn}}:3(1,0,0), J_6^{\text{Mn}}:3(0,0,1)$
Ni1(2d)	2	(1/2,0,0)	$J_1:1(0,1,0), J_2:1(0,0,0), J_3:3(0,0,0), J_4^{\text{Ni}}:1(1,0,0), J_5^{\text{Ni}}:1(0,1,0), J_6^{\text{Ni}}:4(0,0,1), J_6^{\text{Ni}}:4(-1,0,0), J_6^{\text{Ni}}:4(0,0,0), J_6^{\text{Ni}}:4(-1,0,1)$
Mn2(2c)	3	(1/2,0,1/2)	$J_1:4(0,1,0), J_2:4(0,0,0), J_3:2(0,0,0), J_4^{\text{Mn}}:3(1,0,0), J_5^{\text{Mn}}:3(0,1,0), J_6^{\text{Mn}}:1(0,0,0), J_6^{\text{Mn}}:1(-1,0,-1), J_6^{\text{Mn}}:1(-1,0,0), J_6^{\text{Mn}}:1(0,0,-1)$
Ni2(2d)	4	(0,1/2,1/2)	$J_1:3(1,0,0), J_2:3(0,0,0), J_3:1(0,0,0), J_4^{\text{Ni}}:4(1,0,0), J_5^{\text{Ni}}:4(0,1,0), J_6^{\text{Ni}}:2(1,0,0), J_6^{\text{Ni}}:2(0,0,-1), J_6^{\text{Ni}}:2(0,0,0), J_6^{\text{Ni}}:2(1,0,-1)$

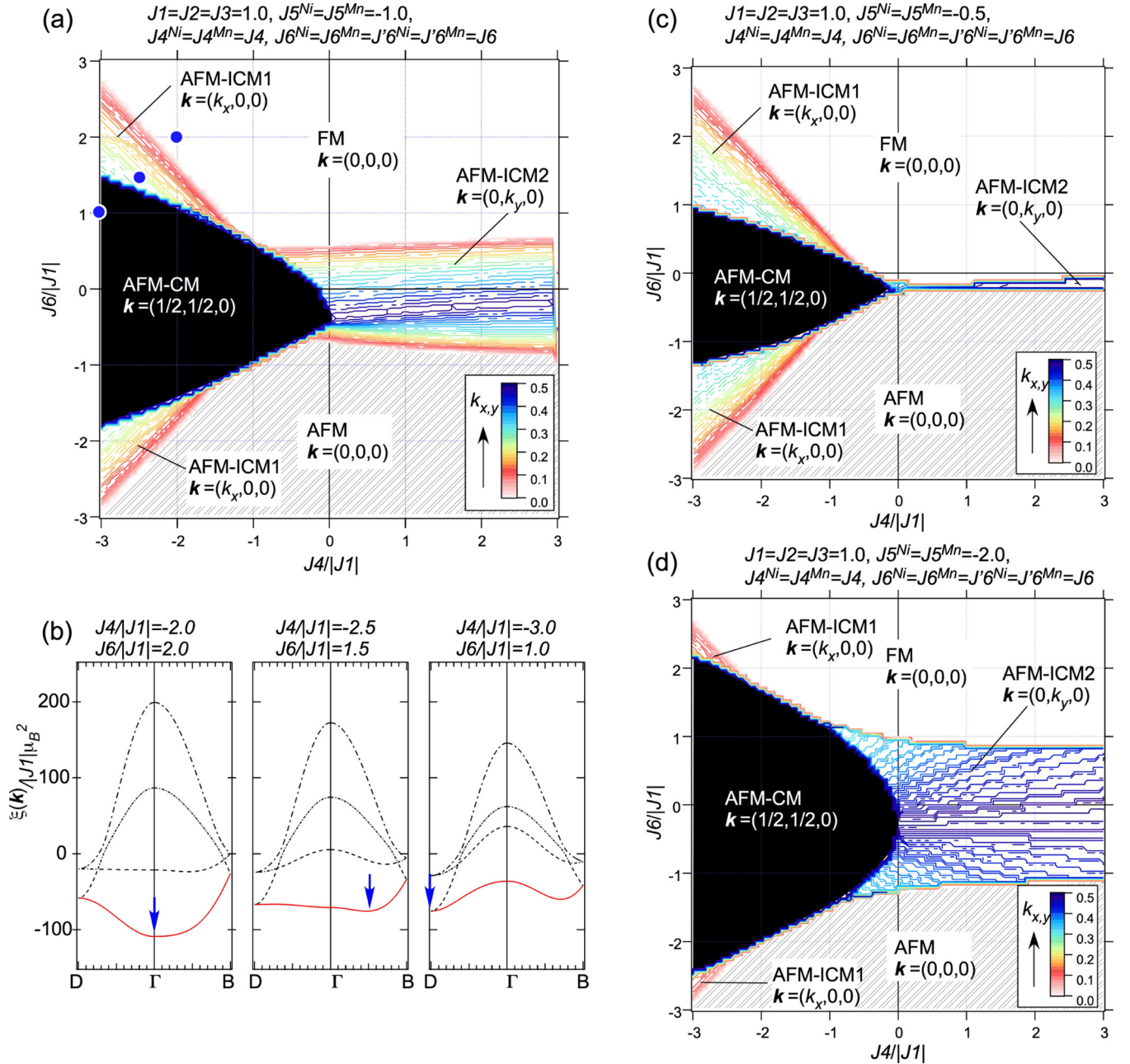


FIG. 9. (a) Magnetic phase diagram representing the stability of different states in the case when $J_1 = J_2 = J_3 = 1.0$, $J_4^{\text{Ni}} = J_4^{\text{Mn}} = J_4$, $J_5^{\text{Ni}} = J_5^{\text{Mn}} = -1.0$, and $J_6^{\text{Ni}} = J_6^{\text{Mn}} = J_6$. The color scale denotes an incommensurability in the propagation vectors, $\mathbf{k} = (k_x, 0, 0)$ and $\mathbf{k} = (0, k_y, 0)$. (b) Dispersion relations for the eigenvalues of the exchange matrix, Eq. (1), for the sets of J -parameters indicated by the filled circles in (a), along directions connecting special points, $D = (\frac{1}{2}, \frac{1}{2}, 0)$, $\Gamma = (0, 0, 0)$, and $B = (\frac{1}{2}, 0, 0)$, in the first Brillouin zone of the $P2_1/n$ space group. (c) and (d) Magnetic phase diagrams for the other cases with $J_5 = -0.5$ in (c) and $J_5 = -2.0$ in (d) and the other J -parameters are the same as (a).

for three NN interactions do not significantly change by application of pressure in LNMO. The NN bond angles in LNMO are similar to the FM case of Y_2NiMnO_6 . This implies that the Ni-O-Mn interactions are also FM, even at $P = 6.0$ GPa in LNMO. Although the signs of the NNN interactions are unknown, we expect that some of them are AFM due to the emergence of AFM order in the high-pressure region in LNMO.

To roughly explain why the ground state in LNMO is changed from FM ordering to AFM ordering with the ICM

propagation vector, we calculate magnetic ground states by mean-field theory. We calculate the negative Fourier transformation of the exchange integrals matrix:

$$\xi_{ij}(\mathbf{k}) = - \sum_{ij=1}^4 E_{ij}(\mathbf{R}_{ij}) \exp\{-2\pi i \mathbf{k} \cdot \mathbf{R}_{ij}\},$$

$$E_{ij} = J_{ij}(\mathbf{S}_i \cdot \mathbf{S}_j). \quad (1)$$

Here, J_{ij} is the exchange integral for two spins, S_i and S_j , and \mathbf{R}_{ij} is a position vector connecting i and j sites. The spins are placed in the unit cell as (1) Mn1(0,0.5,0), (2) Ni1(0.5,0,0), (3) Mn2(0.5,0,0.5), and (4) Ni2(0,0.5,0.5), as illustrated in Fig. 8. The possible NN and NNN exchange bonds are illustrated in Fig. 8 and are listed in Table II. The exchange matrix can be written as follows:

$$\xi_{ij}(\mathbf{k}) = -2 \begin{pmatrix} \xi_{11} & \xi_{12} & \xi_{13} & \xi_{14} \\ \xi_{12} & \xi_{22} & \xi_{14} & \xi_{24} \\ \xi_{13} & \xi_{14} & \xi_{11} & \xi_{12} \\ \xi_{14} & \xi_{24} & \xi_{12} & \xi_{22} \end{pmatrix},$$

$$\xi_{11} = J_4^{\text{Mn}} S_{\text{Mn}}^2 \cos(2\pi k_x) + J_5^{\text{Mn}} S_{\text{Mn}}^2 \cos(2\pi k_y),$$

$$\xi_{12} = S_{\text{Mn}} S_{\text{Ni}} [J_1 \cos\{\pi(k_x - k_y)\} + J_2 \cos\{\pi(k_x + k_y)\}],$$

$$\xi_{13} = J_6^{\text{Mn}} S_{\text{Mn}}^2 [\cos\{\pi(k_x + k_y + k_z)\} \\ + \cos\{\pi(k_x - k_y + k_z)\} \\ + J_6^{\text{Mn}} S_{\text{Mn}}^2 [\cos\{\pi(k_x - k_y - k_z)\} \\ + \cos\{\pi(k_x + k_y - k_z)\}],$$

$$\xi_{14} = J_3 S_{\text{Mn}} S_{\text{Ni}} \cos(\pi k_z),$$

$$\xi_{22} = J_4^{\text{Ni}} S_{\text{Ni}}^2 \cos(2\pi k_x) + J_5^{\text{Ni}} S_{\text{Ni}}^2 \cos(2\pi k_y),$$

$$\xi_{24} = J_6^{\text{Ni}} S_{\text{Ni}}^2 [\cos\{\pi(k_x + k_y + k_z)\} \\ + \cos\{\pi(k_x - k_y + k_z)\} \\ + J_6^{\text{Ni}} S_{\text{Ni}}^2 [\cos\{\pi(k_x - k_y - k_z)\} \\ + \cos\{\pi(k_x + k_y - k_z)\}].$$

Here, we consider the simple case with $J_1 = J_2 = J_3 \equiv J_1 > 0$, $J_4^{\text{Ni}} = J_4^{\text{Mn}} \equiv J_4$, $J_5^{\text{Ni}} = J_5^{\text{Mn}} \equiv J_5$, $J_6^{\text{Ni}} = J_6^{\text{Mn}} \equiv J_6$. The magnitudes of the spins are also assumed to be $S_{\text{Mn}} = 3\mu_B$ for Mn^{4+} and $S_{\text{Ni}} = 2\mu_B$ for Ni^{2+} in this calculation. To find the most stable magnetic ordering for each set of J_{ij} , we numerically diagonalize the matrix using the program ENERMAG [30].

The magnetic phase diagram as functions of J_4 and J_6 in $J_5 = -1.0$ is shown in Fig. 9(a). There is one FM and four AFM phases that include AFM-CM1 [$\mathbf{k} = (1/2, 1/2, 0)$], AFM-CM2 [$\mathbf{k} = (0, 0, 0)$], AFM-ICM1 [$\mathbf{k} = (k_x, 0, 0)$], and AFM-ICM2 [$\mathbf{k} = (0, k_y, 0)$] phases. As shown by the three dots in the phase diagram, the phase transition from a FM phase to an AFM-CM phase through an AFM-ICM phase, which is experimentally seen in A_2NiMnO_6 with changing ionic radius for $A = \text{Lu-In-Sc}$ and application of pressure in $\text{Lu}_2\text{NiMnO}_6$, can be qualitatively reproduced by a slight change in the ratio J_6/J_4 . The phase diagrams for the other two cases for $J_5 = -0.5$ and -2.0 are shown in Figs. 9(c) and 9(d). The overall features of these two cases are similar to the case of $J_5 = -1.0$ [Fig. 9(a)], apart from reducing and enlarging the area of the AFM-CM and AFM-ICM phases. In the calculation, we did not find solutions with experimentally

observed $\mathbf{k} = (k_x, 0, k_z)$ in $\text{In}_2\text{NiMnO}_6$ and one of the possibilities for the high-pressure phase of $\text{Lu}_2\text{NiMnO}_6$, and the multi- \mathbf{k} in $\text{Sc}_2\text{NiMnO}_6$. The reason for this may be that the assumption on the exchange interaction parameters is simplified too much. A further theoretical calculation is needed to understand the exchange parameters in A_2NiMnO_6 .

Dispersion relations for the eigenvalues in Eq. (1) are shown in Fig. 9(b) for the cases indicated by the three dots in Fig. 9(a). The lowest branches in the three cases have relatively flat dispersions compared with the full bandwidths corresponding to the overall exchange interaction. This indicates that the exchange interactions are strongly competing with each other. We thus find that a slight modification of the delicate balance of the competing NNN exchange interactions— J_4 , J_5 , and J_6 —plays an important role for the FM \leftrightarrow AFM-ICM \leftrightarrow AFM-CM phase transitions in A_2NiMnO_6 .

V. CONCLUSION

To study the phase transition from FM to AFM phases in the double perovskite A_2NiMnO_6 , we have investigated the influence of pressure on magnetic order for $\text{Lu}_2\text{NiMnO}_6$ by magnetization, magnetic susceptibility measurements, and neutron diffraction experiments under high pressure up to $P = 8.0$ GPa. In the macroscopic measurements, the FM correlation is significantly suppressed, and the phase-transition temperature is lowered by application of pressure. In the neutron diffraction experiment, we have determined the magnetic structure at ambient pressure, which is the simple FM ordering with Ni and Mn spins in the ac -plane. The FM long-range order at ambient pressure disappears above 4.5 GPa. In the high-pressure phase, the AFM ordering with the ICM \mathbf{k} -vector is induced, which is similar to the case of $\text{In}_2\text{NiMnO}_6$ [13]. From the mean-field calculation, we infer that slight modification of the delicate balance of the competing NNN exchange interactions— J_4 , J_5 , and J_6 —plays an important role for the emergence of the FM \leftrightarrow AFM-ICM \leftrightarrow AFM-CM phase transitions in A_2NiMnO_6 .

ACKNOWLEDGMENTS

The images shown in Figs. 5 and 8 were drawn using the VESTA [31] software program developed by K. Momma. The neutron diffraction experiment was performed with the approval and support of the Institut Laue Langevin [32]. This work was supported by JSPS KAKENHI Grants No. 15H05433, No. 17KK0099, and No. 19H00648, and JST-Mirai Program Grant No. JPMJMI18A3, Japan. A.A.B. acknowledges JSPS KAKENHI Grant No. JP20H05276, a research grant (40-37) from Nippon Sheet Glass Foundation for Materials Science and Engineering, and Innovative Science and Technology Initiative for Security (Grant No. JPJ004596) from Acquisition, Technology, and Logistics Agency (ATLA), Japan.

[1] F. K. Patterson, C. W. Moeller, and R. Ward, *Inorg. Chem.* **2**, 196 (1963).

[2] F. S. Galasso, F. C. Douglas, and R. J. Kasper, *J. Chem. Phys.* **44**, 1672 (1966).

- [3] T. Nakagawa, *J. Phys. Soc. Jpn.* **24**, 806 (1968).
- [4] K.-I. Kobayashi, T. Kimura, H. Sawada, K. Terakura, and Y. Tokura, *Nature (London)* **395**, 677 (1998).
- [5] D. Choudhury, P. Mandal, R. Mathieu, A. Hazarika, S. Rajan, A. Sundaresan, U. V. Waghmare, R. Knut, O. Karis, P. Nordblad, and D. D. Sarma, *Phys. Rev. Lett.* **108**, 127201 (2012).
- [6] T. Kimura, T. Goto, H. Shintani, K. Ishizaka, T. Arima, and Y. Tokura, *Nature (London)* **426**, 55 (2003).
- [7] S.-W. Cheong and M. Mostovoy, *Nat. Mater.* **6**, 13 (2007).
- [8] Y. Tokura and S. Seki, *Adv. Mater.* **22**, 1554 (2010).
- [9] J. Blasco, J. L. Garcia-Munoz, J. Garcia, J. Stankiewicz, G. Subias, C. Ritter, and A. Rodriguez-Velamazán, *Appl. Phys. Lett.* **107**, 012902 (2015).
- [10] S. Yáñez-Vilar, E. D. Mun, V. S. Zapf, B. G. Ueland, J. S. Gardner, J. D. Thompson, J. Singleton, M. Sánchez-Andújar, J. Mira, N. Biskup, M. A. Señañis-Rodríguez, and C. D. Batista, *Phys. Rev. B* **84**, 134427 (2011).
- [11] W. Yi, Q. Liang, Y. Matsushita, M. Tanaka, and A. A. Belik, *Inorg. Chem.* **52**, 14108 (2013).
- [12] A. A. Belik and W. Yi, *J. Phys.: Condens. Matter* **26**, 163201 (2014).
- [13] N. Terada, D. D. Khalyavin, P. Manuel, W. Yi, H. S. Suzuki, N. Tsujii, Y. Imanaka, and A. A. Belik, *Phys. Rev. B* **91**, 104413 (2015).
- [14] W. Yi, A. J. Princep, Y. Guo, R. D. Johnson, D. Khalyavin, P. Manuel, A. Senyshyn, I. A. Presniakov, A. V. Sobolev, Y. Matsushita, M. Tanaka, A. A. Belik, and A. T. Boothroyd, *Inorg. Chem.* **54**, 8012 (2015).
- [15] J. B. Goodenough, *Phys. Rev.* **100**, 564 (1955); *Magnetism and the Chemical Bond* (Interscience, New York, 1963).
- [16] J. Kanamori, *J. Phys. Chem. Solids* **10**, 87 (1959).
- [17] K. Asai, K. Fujiyoshi, N. Nishimori, Y. Sutoh, Y. Kobayashi, and M. Mizoguchi, *J. Phys. Soc. Jpn.* **67**, 4218 (1998).
- [18] K. Asai, N. Kobayashi, T. Bairo, N. Kaneko, Y. Kobayashi, M. Suzuki, Y. Satoh, and M. Mizoguchi, *J. Phys. Soc. Jpn.* **74**, 1289 (2005).
- [19] R. J. Booth, R. Fillman, H. Whitaker, A. Nag, R. M. Tiwari, K. V. Ramanujachary, J. Gopalakrishnan, and S. E. Lofland, *Mater. Res. Bull.* **44**, 1559 (2009).
- [20] S. Kumar, G. Giovannetti, J. van den Brink, and S. Picozzi, *Phys. Rev. B* **82**, 134429 (2010).
- [21] H. Nhalil, H. S. Nair, C. M. N. Kumar, A. M. Strydom, and S. Elizabeth, *Phys. Rev. B* **92**, 214426 (2015).
- [22] J. Oliveira, J. Agostinho Moreira, A. Almeida, V. H. Rodrigues, M. M. R. Costa, P. B. Tavares, P. Bouvier, M. Guennou, and J. Kreisel, *Phys. Rev. B* **85**, 052101 (2012).
- [23] N. Mori, H. Takahashi, and N. Takeshita, *High Press. Res.* **24**, 225 (2004).
- [24] T. Hansen, P. F. Henry, H. E. Fischer, J. Torregrossa, P. Convert, and H. A. Convert, *Meas. Sci. Technol.* **19**, 034001 (2008).
- [25] S. Klotz, T. Hansen, E. Lelièvre-Berna, L. Amand, J. Maurice, and C. Payre, *J. Neutron Res.* **21**, 117 (2019).
- [26] J. Rodriguez-Carvajal, *Physica B* **192**, 55 (1993).
- [27] R. I. Dass, J.-Q. Yan, and J. B. Goodenough, *Phys. Rev. B* **68**, 064415 (2003).
- [28] I. Maartense and G. Williams, *Phys. Rev. B* **17**, 377 (1978).
- [29] B. J. Campbell, H. T. Stokes, D. E. Tanner, and D. M. Hatch, *J. Appl. Crystallogr.* **39**, 607 (2006).
- [30] N. El Khayati, R. C. El Moursli, J. Rodriguez-Carvajal, G. Andre, N. Blanchard, F. Bouree, G. Collin, and T. Roisnel, *Eur. Phys. J. B* **22**, 429 (2001).
- [31] K. Momma and F. Izumi, *J. Appl. Crystallogr.* **41**, 653 (2008).
- [32] N. Terada, C. V. Colin, T. Hasen, and N. Qureshi, Investigation of pressure-induced ferromagnetic to spiral phase transition in a multiferroic double-perovskite $\text{In}_2\text{NiMnO}_6$, Institut Laue-Langevin (ILL), doi:10.5291/ILL-DATA.5-31-2640.